An unusual radiation dose dependent EPR line at g_{eff} = 2.54 in feldspars: possible evidence of $Fe^{3+}O^{2-} \leftrightarrow Fe^{2+}O^{-}$ and exchange coupled Fe^{3+}–Fe^{2+}–nO^{-}

2008 J. Phys.: Condens. Matter 20 025224

(http://iopscience.iop.org/0953-8984/20/2/025224)

J. Phys.: Condens. Matter **20** (2008) 025224 (9pp) doi:10.1088/0953-8984/20/02/025224

An unusual radiation dose dependent EPR line at $g_{\mathrm{eff}} = 2.54$ in feldspars: possible evidence of $Fe^{3+}O^{2-} \leftrightarrow Fe^{2+}O^{-}$ and exchange coupled Fe^{3+}–Fe^{2+}–nO^{-}

M D Sastry[1], Y C Nagar[1], B Bhushan[2], K P Mishra[3], V Balaram[4] and A K Singhvi[1,5]

[1] Physical Research Laboratory, Navrangpura, Ahmedabad, 380 009, India
[2] Food Technology Division, Bhabha Atomic Research Center, Trombay, Mumbai, 400 085, India
[3] Radiation Biology and Health Sciences, Bhabha Atomic Research Center, Mumbai, 400 085, India
[4] Geochemistry Division, National Geophysical Research Institute, Hyderabad, 500 007, India

E-mail: singhvi@prl.res.in

Received 7 April 2007, in final form 22 October 2007
Published 13 December 2007
Online at stacks.iop.org/JPhysCM/20/025224

Abstract

We report electron paramagnetic resonance (EPR) results on natural feldspar grains extracted from sediment samples of three widely different source regions. The XRD analysis indicated that the samples had albite, microcline and Ca/Ba–orthoclase as the major constituents. The EPR spectrum of all the samples exhibited an intense line around $g_{\mathrm{eff}} = 4.3$. This is characteristic of Fe^{3+} with a zero field splitting that is significantly larger than the microwave quantum. More interesting was the presence of a strong EPR signal in the region of $g_{\mathrm{eff}} = 2.54$–2.7. On irradiation with gamma rays the position of the line shifted to higher magnetic field. The possible origin of this line and its unusual behavior with dose is explained as being due to the interaction of a hopping 'hole' on oxygen with iron centers. The possibilities considered include (1) the valence fluctuation of an Fe^{3+} center at a tetrahedral site, (2) oscillation of FeO_4^- between two resonant forms, $Fe^{2+}O^-$ and $Fe^{3+}O^{2-}$, and (3) exchange coupling between Fe^{3+}, Fe^{2+} and O^-. The concentration of the latter is dose dependent and, consequently, it results in the observed dose dependent line shift.

1. Introduction

Feldspars, the alkali aluminosilicates ($Na/KAlSi_3O_8$), are ubiquitous minerals in the Earth's crust. Sanidine and orthoclase (potassium feldspar) have the monoclinic structure while plagioclases (sodium/calcium feldspar) have a triclinic structure. Smaller ions, Si^{4+} and Al^{3+}, take the tetrahedral sites (four T-sites designated as T1(O), T1(m), T2(O), and T2(M)). Larger alkali ions, Na^+ and K^+, occupy irregular cavities in the tetrahedral framework (M-sites) [1, 2]. An understanding of the positional order–disorder of Al^{3+} and Si^{4+} among the tetrahedral sites in alkali feldspars is of interest, from the basic structural point of view and for their role in disorder induced electron/hole traps [3–5]. Within the feldspar matrix, the extent of order is also expected to serve as an indicator of fluid–rock interaction [6].

In the plagioclase series, a complete range of compositions exists. These range between the aluminosilicates of sodium and an alkaline earth element (Ca). Various trace level impurities such as Fe (both as ferrous and ferric), rare-earth elements, Mn, Pb, Ge, Ti etc also get incorporated [2]. Fe^{3+} is tetrahedrally coordinated in both plagioclase and disordered K feldspars and Fe^{2+} occupies only the M-sites in plagioclase. The concentration of calcium decides the partitioning of iron in plagioclase [4]. Interplay of the order–disorder and the point

[5] Author to whom any correspondence should be addressed.

Table 1. EPR of Fe^{3+} related centers reported in feldspars.

g_{eff}	Assignment	Reference	Comments
1.8	Clusters of magnetically interacting Fe^{3+} ions	Speit and Lehman [4]	—
2.3	Haematitic formation (clusters of magnetically interacting iron)	Hoffmeister and Rossman [5]	A broad band at $g_{eff} = 2.18$ was also observed. It was not assigned to magnetically interacting iron; it was assigned to a radiation damage center modeled by Griscom [34].
2.0	Iron clusters T1	Hoffmeister and Rossman [5]	
3.3 (isotropic), 5.9, 7.1, 12.2, 15	Axially coordinated Fe^{3+}	Hoffmeister and Rossman [5]	HR proposed that $g_{eff} = 3.3$ is due to an axially coordinated Fe^{3+}, representing an intermediate stage in the deposition of haematite in the feldspars, *but it is not haematite itself*.
4.3 (isotropic)	Fe^{3+} at regular tetrahedral sites (T10)	Petrov *et al* [27], Finch and Klein [7]	The extent of order can be inferred from $g = 4.3$ and 3.7 lines only in single crystal samples. In powder samples parallel features at $g = 3.7$ will be too weak, and the $g = 4.3$ line will have contributions from both sites.
3.7 ($\parallel$), 4.3 ($\perp$)	Fe^{3+} at disordered sites		

defects in the feldspar lattice, that can accommodate metal ion impurities (particularly those exhibiting multiple valences), appears to be the basic cause of the high luminescence sensitivity of feldspars. However, such a complex system is also associated with numerous problems, that make their use in routine radiation dosimetric and geochronological application non-trivial. The presence of iron impurity in almost all feldspars and the amenability of Fe^{3+} ion (an S-state ion with $3d^5$ outer electron configuration) for electron paramagnetic resonance (EPR) investigations have been used for investigating the order–disorder in feldspars [3–7]. EPR results on Fe^{3+} in alpha-quartz (with a site symmetry at Fe^{3+} similar to that in feldspars) have aided these studies. Thus, the early work of Weil *et al* on EPR of Fe^{3+} at Si^{4+} sites in alpha-quartz and the centers associated with charge compensating alkali ions elucidated the dynamics of Fe^{3+} and its correlation with hole hopping at the FeO_4^- complex [8–13]. Table 1 summarizes the EPR of Fe^{3+} related centers reported in feldspars. The problems of current interest in feldspars relate to the extent of order and the anomalous decay of luminescence.

1.1. The extent of order in feldspar

The intensity of the $g = 4.3$ EPR line of Fe^{3+} in feldspars is widely used to assess the positional order in feldspar samples. Due to an interesting coincidence of admixture of Kramers' doublets of the ^6S state of Fe^{3+} in a strong crystal field, a slightly anisotropic line around $g = 4.3$ is reported in a number of widely different matrices such as borosilicate glasses and biological systems [14–17]. The implication of this observation is that this line is not unique to Fe^{3+} at tetrahedral sites, and definitive conclusions on the site symmetry of ferric iron cannot be drawn using powder samples. A workable and a reliable criterion for assessing the extent of order in feldspars using the EPR of Fe^{3+} in powder samples is therefore needed.

1.2. Anomalous decay of luminescence

Anomalous decay of luminescence from deep traps has been enigmatic and despite several studies its proper elucidation (to the extent of the estimation and correction of decay rates), is not yet available. An understanding of the physical properties of unpaired electrons (both localized and itinerant if any (e.g. hopping O^-)) in the matrix, is needed to obtain a greater insight into the luminescence process and the mechanisms of its thermal/athermal decay.

In this contribution, the results of room temperature EPR measurements on six feldspar samples from three different locations (namely USA, Canada, and China), are presented. Interesting EPR evidence is presented to suggest interaction between iron impurities and mobile holes on oxygen.

2. Experimental details

2.1. Sample detail, provenances and characterization

Samples from USA and Canada (designated as GP-3, Y7A, and TML-1 respectively) were coarse grained ($\sim$100 μm); samples from China (Dz-2, Dz-4, DzN-1) were polymineralic fine grained (4–11 μm) aeolian dust samples. Sample GP-3 was from the Pliocene Yorktown Formation exposed at the Gomez Pit, Virginia, USA; TML-1 was from the Pliocene unit exposed at the Ch'ijee's Bluffs, Yukon, Canadian Cordillera; Y7A was a beach sand from Lake Erie, Ontario, Canada.

Extraction of clean feldspar grains from these rocks/sediments comprised pretreatment with 1 N HCl and 30% H_2O_2 (to remove carbonates and organic matter) and sodium polytungstate (<2.58 gm cm^{-3}) heavy density separation. X-ray diffraction (XRD) analysis indicated the dominance of feldspar components, i.e. albite and orthoclase (table 2), in the grain separates and aeolian dust samples. In these samples, Fe impurity ranged from 0.16 to 4.19% and rare-earth

Table 2. The mineral composition of 'feldspar' samples investigated as obtained by XRD analysis.

sample	Mineral compositions	% composition	Chemical composition
Aeolian dust	Quartz	50	SiO_2
	Albite	∼30	$NaAlSi_3O_8$
	Muscovite	∼20	$KAl_2(AlSi_3O_{10})(OH)_2$
Gp-3	Orthoclase	∼15	$KAlSi_3O_8$
	Albite (Ca ordered)	∼9	$(Na,Ca)AlSi_3O_8$
	Microline	∼60	$KAlSi_3O_8$
	Orthoclase sodium	∼9	$K_{0.58}Na_{0.42}AlSi_3O_8$
	Vermiculite	∼7	$Mg_{3.4}Si_{2.9}Al_{1.14}O_{10}(OH)_2(H_2O)_{3.72}$
Y7A	Microline	∼54	$K_{0.94}Na_{0.06}Al_{1.01}Si_{2.99}O_8$
	Albite	∼11	$Na(AlSi_3O_8)$
	Orthoclase	∼26	$K_{0.59}Ba_{0.19}Na_{0.22}(Al_{1.18}Si_{2.82}O_8)$
	Quartz	∼9	SiO_2
TML-1	Anorthoclase (disordered)	∼10	$(Na,K)Si_3AlO_8$
	Albite	∼20	$(Na,Ca)AlSi_3O_8$
	Microcline (intermediate)	∼70	$K_{0.89}Na_{0.1}Ba_{0.01}Al_{0.99}Si_{3.01}O_8$

elements, particularly Gd, ranged from the 0.22 ppm to the 4.3 ppm level, also reported earlier [18].

The above values are based on ICP-MS multielement analysis at the National Geophysical Research Institute, Hyderabad. The sample preparation and ICP-MS analysis involved digestion of the weighed sample (∼0.05 g) in Savillex Teflon pressure decomposition vessels. To each sample, 10 ml of an acid mixture containing a 7:3:1 ratio of HF:HNO_3 and $HClO_4$ were added along with 1 ml of HCl. The vessels were sealed and placed in an electric oven at 110 °C for five days. The vessels were then cooled to room temperature and the contents were evaporated to near dryness on a hot plate. The evaporation process was repeated after adding 5 ml of the above acid mixture. Finally, the residue was dissolved in 20 ml of 1:1 HNO_3 with gentle heating. Clear solutions were obtained for all samples. After cooling to room temperature, the volume was made up to 250 ml, transferred to 60 ml polyethylene bottles and analyzed by ICP-MS. Rhodium was used as internal standard. The calibration of the instrument was carried out using 0.02% solution of JB-2, a Japanese basaltic rock reference material. A French anorthosite reference sample solution (ANG) was used to check the accuracy of the analysis. Other details of the analytical procedure, instrumentation and data acquisition are given by Zahida *et al* [19]. ICP-MS results are given in tables 3(a) and (b).

2.2. EPR measurements

Room temperature EPR measurements were carried out on a Bruker ELEXYS Emx6/1 X-band EPR spectrometer, at microwave powers of 0.1, 1.0 and 5 mW and modulation amplitude of 1 G. As some samples contained quartz (see table 2), microwave power levels of >1 mW were used to ensure saturation of signals from quartz based centers [16]. The signals of transition metal ions, Fe and Mn were investigated at 5 mW. The samples and measurements were handled in subdued red light conditions that are typical of a luminescence dating laboratory. This was to avoid any photo-transfer effects due to daylight exposure.

3. Results

The geochemical analysis (tables 3(a) and (b)) indicates values typical of feldspars. The EPR spectrum of all the samples comprised typical feldspar lines at effective g-values, $g_{\text{eff}} = 4.3$ and other sample dependent signals. In addition, an intense line around $g_{\text{eff}} = 2.54$ was observed for the first time. The line position shifted to higher fields (lower g-values) with increasing radiation dose. Such a dependence of line position on radiation dose is rare, and provides a means to understand the interaction of itinerant electrons with static paramagnetic centers. We suggest the following.

(1) The line at $g_{\text{eff}} = 2.54$ is due to interaction of mobile oxygen hole centers with static Fe^{2+}/Fe^{3+}.
(2) The dose dependence of line position is the manifestation of increasing number of oxygen hole centers with dose.
(3) The observation of the $g_{\text{eff}} = 2.54$ line has implications for the reported cyclotron resonance in potassium feldspars [20] and will be dealt with elsewhere.

3.1. Feldspar grain separates

The EPR spectra of all the three natural (as received) samples contained an intense line at $g = 4.3$, a sharp and intense line at $g_{\text{eff}} = 2.545$, a broad feature with peak position around 3 kG ($g = 2.33$) and other lines at lower fields ($g > 2.3$).

3.1.1. Sample Y7A. Figures 1(a)–(c) show the EPR of the sample, (a) as received (i.e. only with its natural (geological) dose N), (b) after a 200 Gy ^{60}Co-gamma dose, i.e. with a total dose of ($N + 200$ Gy) and (c) after an additional gamma dose of 200 Gy, i.e. with a total dose of ($N + 400$ Gy). A sharp line marked 'X' at 2750 G, corresponding to $g_{\text{eff}} = 2.545$, was seen in samples as received. Lines at $g = 4.53$, 4.3, 3.3,

Table 3. ICP-MS results on four feldspar samples.

(a)

Element	GP-3 (ppm)	Dz-2 (ppm)	TML-1 (ppm)	Y7A (ppm)	ANG[a] This study	ANG[a] Reported value
Sc	2.90	9.61	2.31	2.24	9.80	10.00
V	12.74	68.21	11.32	10.60	69.77	70.00
Cr	129.70	60.80	51.41	27.90	50.22	50.00
Mn	40	720	20	20	400	400
Co	1.33	9.90	1.61	0.70	25.13	25.00
Ni	43.20	36.23	24.34	17	35	35.00
Cu	8.98	25.32	6.91	6.78	18.90	19.00
Zn	18.50	39.71	14.60	37.50	19.82	20.00
Ga	14.20	12.50	10.70	13.64	17.92	18.00
Rb	189	73	448	237	0.98	1.00
Sr	399	267	141	291	75.67	76.00
Y	1.01	20.30	2.47	1.12	7.50	7.50
Zr	26.50	139.70	25.12	16.90	10.90	11.00
Nb	0.91	6.80	0.64	0.65	0.71	0.70
Cs	1.43	6.90	11.43	2.59	0.05	0.05
Ba	2000	317	713	1948	34.23	34.00
La	4.53	27.33	4.00	3.78	2.24	2.20
Ce	5.12	55.40	6.67	4.30	4.67	4.70
Pr	0.47	6.48	0.71	0.67	0.58	0.60
Nd	1.54	22.50	2.42	2.12	2.36	2.40
Sm	0.30	5.10	0.53	0.36	0.77	0.70
Eu	1.53	1.03	0.94	0.71	0.37	0.37
Gd	0.22	4.33	0.37	0.27	0.90	0.90
Tb	0.04	0.72	0.07	0.04	0.21	0.20
Dy	0.16	3.57	0.37	0.19	1.21	1.20
Ho	0.03	0.72	0.08	0.04	0.27	0.27
Er	0.10	1.88	0.23	0.10	0.75	0.75
Tm	0.02	0.31	0.04	0.02	0.12	0.12
Yb	0.10	1.82	0.26	0.12	0.72	0.75
Lu	0.02	0.29	0.05	0.02	0.11	0.12
Hf	0.60	3.18	0.62	0.36	0.40	0.38
Ta	0.16	0.90	0.08	0.04	0.17	0.18
Pb	2.82	1.98	3.74	3.17	1.99	2.00
Th	0.10	2.19	0.23	0.09	0.04	0.04
U	0.20	2.36	0.40	0.25	0.13	0.12

(b)

Element	GP-3 (%)	Dz-2 (%)	TML-1 (%)	Y7A (%)	ANG[a] This study	ANG[a] Reported value
Fe	0.64	4.19	0.16	0.16	3.35	3.36

[a] ANG (anorthosite standard from France). Typical measurement precision is ∼5%.

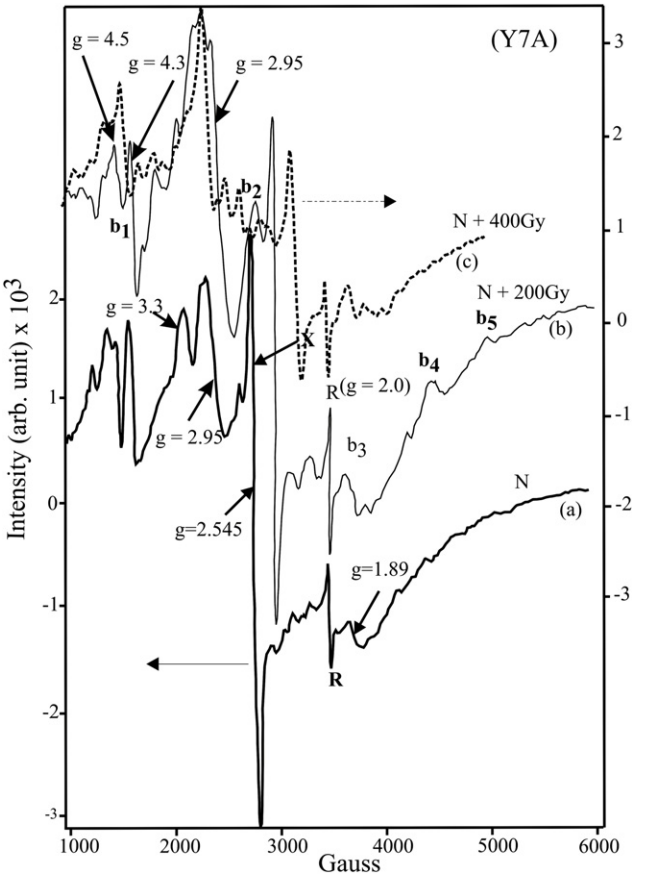

Figure 1. Electron paramagnetic resonance (EPR) spectra of sample Y7A. 30 mg aliquot with (a) zero dose (sample as received), (b) 200 Gy of laboratory gamma dose and (c) a total of 400 Gy of laboratory gamma dose (dashed spectra).

2.95, and 2.00 (marked 'R') and a weak line at $g = 1.89$ were also observed. On gamma irradiation to doses of 200 Gy and 400 Gy, the line marked 'X' shifted to higher fields of 2920 G and 3200 G respectively. The positions of all the other lines remained unaltered. The intensities of some of these lines changed on gamma irradiation; in particular, the peak to peak intensity and width of the line at $g = 2.95$ increased. Further, in gamma irradiated samples, a group of five rather weak lines (marked b1–b5 in figure 1(b)) and a few weaker lines were detected and are discussed in section 4.1. It may be pointed out that no Mn^{2+} signals were clearly observed despite its presence up to a level of 20 ppm. This contrasts with that of TML-1 (see below).

3.1.2. Sample (TML-1). The EPR spectrum of the natural sample (as received) contained the line at $g = 4.3$, a sharp line at $g = 2.00$ and an intense spectrum due to Mn^{2+}, exhibiting a sextet hyperfine structure around $g = 2.00$ (figure 2). This is consistent with the ICP-MS results showing the presence of about 20 ppm Mn. It appears that most of the Mn is in divalent form in this sample. The spectral features of other lines remained unaltered on gamma irradiation to 200 Gy and no additional lines were observed. However, on a 2 h daylight exposure, a line 'X' at $g_{\text{eff}} = 2.545$ appeared. This line shifted from 2750 to 2900 G on gamma irradiation to a dose of 400 Gy (figures 3(a) and (b)).

3.1.3. Sample GP-3. The EPR spectrum of the virgin sample had the line at $g_{\text{eff}} = 2.545$ (in addition to the line at $g = 4.3$) superposed with a broader line with its width spanning from 2550 to 2750 G. The $g_{\text{eff}} = 2.545$ line shifted to higher fields with dose, and the line position after a gamma dose of 400 Gy was at 2850 G. It is interesting to note that this sample did not exhibit EPR of Mn^{2+} despite the fact that ICP-MS results indicated a higher concentration of Mn as compared

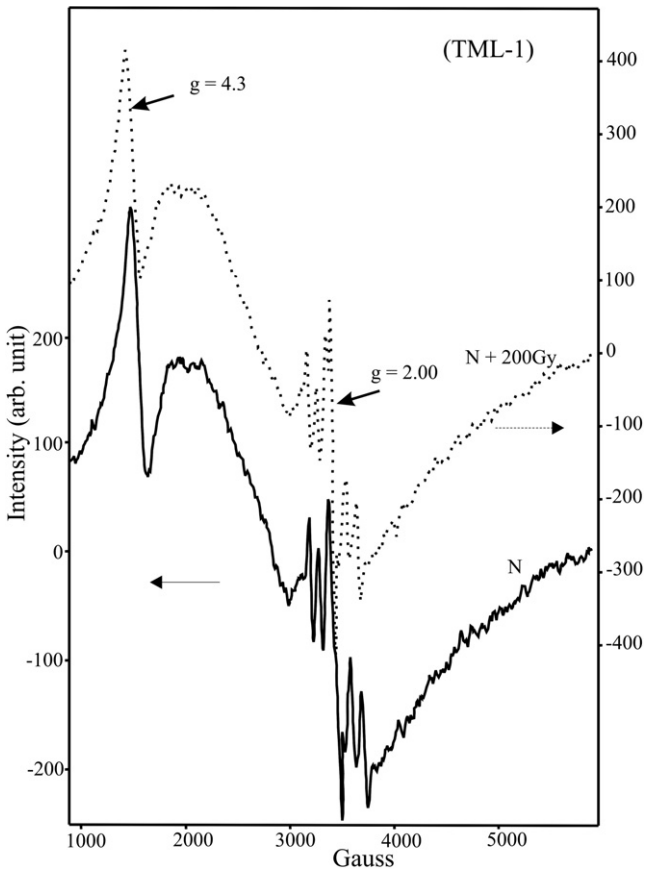

Figure 2. Electron paramagnetic resonance (EPR) spectra of sample TML-1. 30 mg aliquot with zero dose (sample as received) and 200 Gy of gamma dose (dotted spectra).

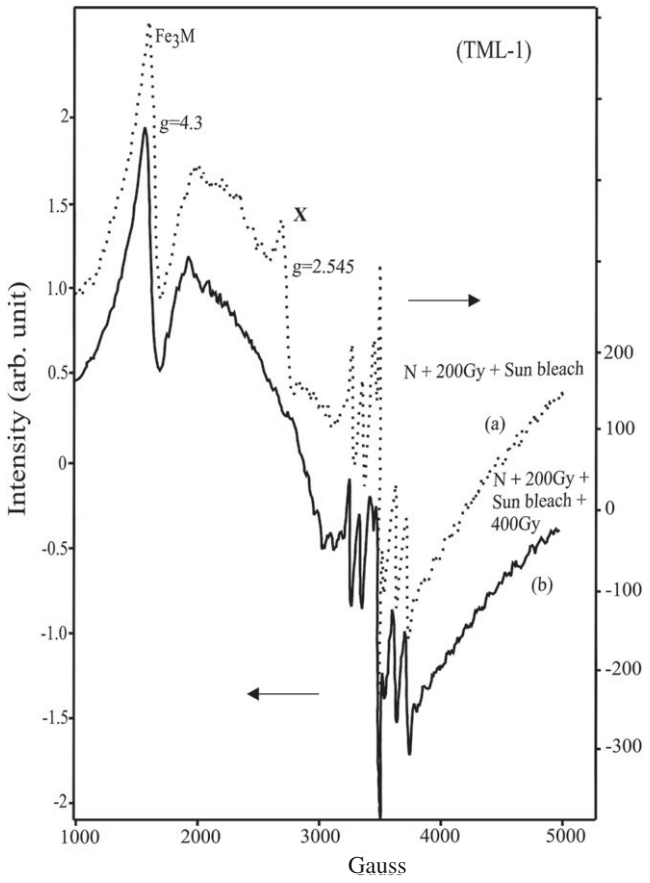

Figure 3. Electron paramagnetic resonance (EPR) spectra of sample TML-1. (a) Sample exposed to sunlight after 200 Gy of gamma dose and (b) sample as in (a), 400 Gy of gamma dose (dotted spectra).

with TML-1. It is possible that the effective valence of Mn may not be 2^+ and/or it is interacting with another paramagnetic species such as O^-.

3.1.4. Aeolian dust sample. The polymineralic, fine grained samples, namely Dz-2, Dz-4, and DzN-1, exhibited a broad and intense line, centered at 2400 G with a peak to peak width of 1200 G, the most intense being that for sample DzN-1. This line suggests the presence of a magnetically ordered impurity phase in the sample. Lines at $g = 5.6$ and 4.3 were superposed on this line. A sharp and intense line was observed at 2672 G ($g_{\text{eff}} = 2.6$) in samples Dz-2 and Dz-4, which shifted to higher fields with external radiation dose (200 Gy). Figure 4 shows the EPR spectrum for Dz-2 in a natural as received sample and the same sample with an additional 200 Gy of gamma dose (N + 200 Gy). The line at $g_{\text{eff}} = 2.6$ shifted to higher field ($g_{\text{eff}} = 2.37$) on gamma irradiation. The dose dependence of the line position was linear in the range 0–400 Gy. Typical dose responses for samples Y7A and Gp-3 are shown in figures 5(a) and (b) respectively.

4. Discussion

The XRD analysis given in table 2 shows that, with the exception of aeolian dust samples, the other four samples predominantly contained alkali feldspars. The aeolian dust samples contained a significant fraction of quartz. The signals with $g_{\text{eff}} = 2.5$–2.6 in all these samples should belong to the feldspar fraction. It is possible that some samples may contain nano-particles of Fe-rich phases. If the nano-particles contained magnetically ordered phases, they would manifest as broad lines or as sharp and intense super-paramagnetic lines around $g = 2.00$. In neither case is a signal with dose dependent line position expected. We thus suggest that the intense and broad signals merely indicate the existence of some magnetically concentrated iron rich phases. The interesting features of the present results are discussed below.

4.1. EPR of Fe^{3+} centers

From amongst the metal ions, the most common metal ions in feldspars are Fe^{3+}, Fe^{2+}, and Mn^{2+}. Amongst these, Fe^{3+} and Mn^{2+} are iso-electronic ($3d^5$) with ^6S ground state. Therefore, due to the long spin–lattice relaxation times characteristic of S-state ions, their EPR could be easily observed at room temperature. Both Fe^{3+} and Mn^{2+} have $g = 2.000$. However, the Fe^{3+} ion often experiences relatively larger crystal field effects such that the separation between the three Kramers' doublets can exceed 0.3 cm^{-1}, the energy of the X-band microwave. In such cases, the five component fine structure

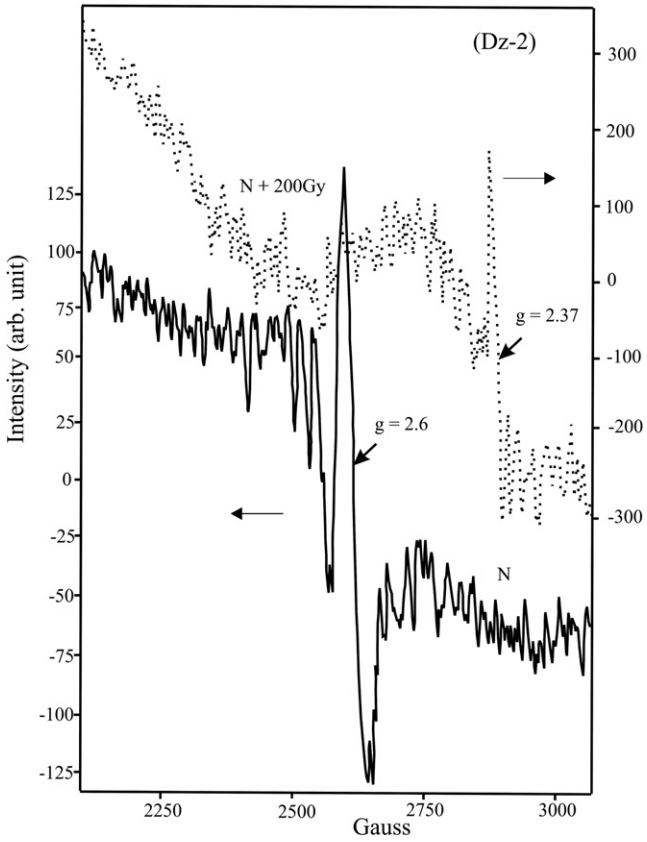

Figure 4. Electron paramagnetic resonance (EPR) spectra of sample Dz-2. 30 mg aliquot with zero dose (sample as received) and 200 Gy of gamma dose (dotted spectra).

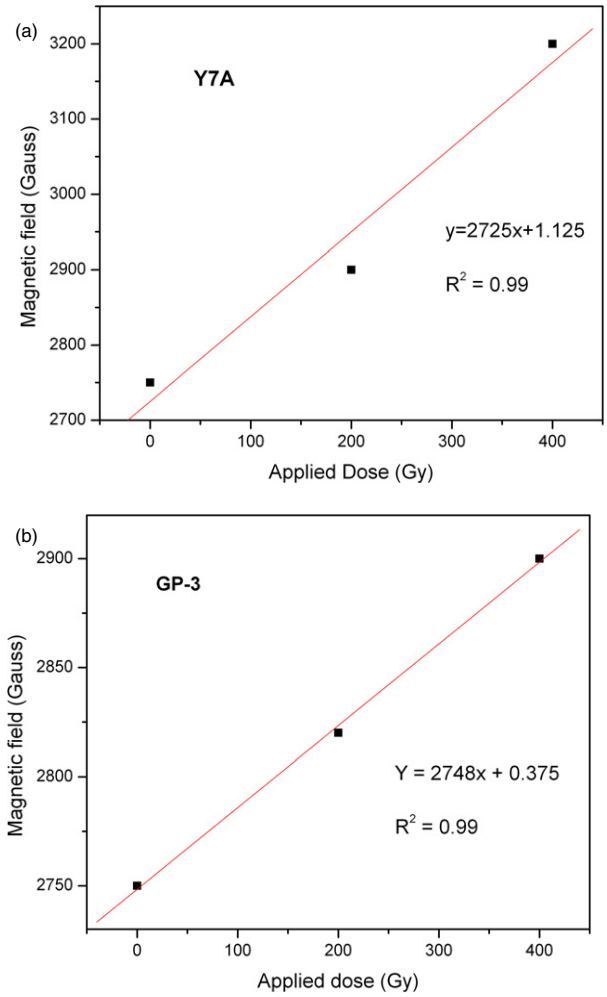

Figure 5. Dose dependence of $g_{\text{eff}} = 2.545$ line position in (a) Y7A sample and (b) GP-3 sample. The errors in magnetic field are smaller than the size of the data points.

(five transitions corresponding to the selection rule $\Delta Ms = \pm 1$) cannot be observed. More often, ESR lines are observed at low fields corresponding to $g_{\text{eff}} \gg 2$, with an isotropic line at $g = 30/7$ (4.28) [15].

In feldspars, the origin of the $g = 4.3$ line of Fe^{3+} is better understood, and has been used to elucidate (Al^{3+}, Si^{4+}) order–disorder over the four distinct tetrahedral positions T1(O), T1(m), T2(O), and T2(m) [5, 6]. In rhombic systems, occurrence of the $g = 4.3$ line is widespread amongst the high spin ferric compounds, including biological crystals such as transferrins and lactoferrins, and is a consequence of symmetry [15–17]. In the tetragonal limit, an isotropic $g = 4.3$ line arises from the relation between fourth degree crystal field parameters (as seen in ferrous tutton salt and ferrous ammonium sulfate), through radiation induced conversion of ferrous to ferric [17]. The iron site in ferrous ammonium sulfate has sixfold coordination with water. In view of the similarity of charge and ionic radii of Al^{3+} and Fe^{3+}, it is expected that the ferric ion goes to a tetrahedral site in all feldspars. A correlation between the intensity of optical absorption of Fe^{3+} at tetrahedral sites and the intensity of the $g = 4.3$ line led Hofmeister and Rossman [5] to establish that the line at $g = 4.3$ was indeed due to Fe^{3+} at tetrahedral sites. Petrov and Hafner [6] investigated the $g = 4.3$ line in sanidine single crystals and identified that the ferric ion at position T1 yields an isotropic line at $g = 4.3$, whereas the line at position T2 has $g = 3.7$ (for magnetic field parallel to the c-axis) and $g = 4.3$ (magnetic field perpendicular to the c-axis). It is important to note that only in the case of single crystals and for $H \parallel c$ can the relative intensities of the lines at $g = 4.3$ and 3.7 be used to assess the occupancy of Fe^{3+} at the respective sites. For powder samples both situations should yield intense lines only at $g = 4.3$, as the parallel component at $g = 3.7$ for the T2 position would be significantly weaker. Clearly then, the inferences based on the relative intensities of the $g = 4.3$ and 3.7 lines in powder samples on Al/Si positional order–disorder from powder spectra [7] would be misleading.

Lines b1–b5, observed only in iron rich samples, are most likely due to Fe^{3+} at nearly regular tetrahedral coordination, wherein it would be possible to observe all five fine structure transitions due to smaller zero field splitting. These became more prominent only with higher radiation dose. The line shape of powder spectra has been discussed previously [15, 21, 22]. Lines b1–b5 have normal 'first-derivative-like' line shape, characteristic of perpendicular components in a powder spectrum. For a weak perpendicular spectrum, parallel components with typical 'bell-like' line shapes would be too weak to be observed. The central $+1/2 \leftrightarrow -1/2$ transition in the perpendicular spectrum (b1–b5) does

not coincide with the $g = 2.00$ position, which probably is due to terms of the type b_4^3 in the spin Hamiltonian [23, 24]. Detailed spectral analysis was not possible, and approximate estimates of the spin Hamiltonian constants g, D, and E in the standard notation are $g = 2.005$, $D \sim 820 \times 10^{-4}$ cm^{-1}, and $E \sim 130 \times 10^{-4}$ cm^{-1}.

It may, however, be remarked that these weaker lines are in no way important to the main focus of the present work, and this brief analysis is presented only for completeness. The lower valence state of iron, Fe^{2+}, is also paramagnetic. Due to fast spin–lattice relaxation, characteristic of orbitally degenerate electronic ground states, EPR of Fe^{2+} can be observed only at very low temperatures. The spectrum of Fe^{2+} was investigated at 4.2 K in the octahedral symmetry of MgO, where its g-value was 3.4277 ± 0.002 [25].

We are not aware of any reports of EPR signals at room temperature with effective $g = 2.5$–3.0. It is difficult to conjecture the existence of any system in silicate materials that would yield such an isotropic g-value. The presence of EPR signals in this region and their position dependence on gamma dose are therefore intriguing. The only possibilities of single line EPR spectra with $g > 2$ are Fe (I), Ni^{3+} and Ni^{+} [15, 26]. However, these species are unlikely to have a g-value of ∼2.5–2.6. The ICP-MS result shows that Fe is present in all samples at per cent level and rare earths in feldspar separates are <5 ppm. Among rare earths it is only Gd^{3+} which can potentially yield an EPR spectrum at RT, without any hyperfine structure (hfs). In the present samples for mineral separates, Gd concentration ranges from 0.22 to 4.33 ppm. The intensity of the spectrum arising from sub-ppm level Gd^{3+} would be distributed among seven fine structure lines per site [15, 22]. In the case of powder samples the intensity would be reduced further, as only the perpendicular spectrum would be observable. As regards the role of Gd^{3+} in the appearance of a single line with $g_{\text{eff}} = 2.545$, it appears least likely that a $4f^7$ ion with $^8S_{7/2}$ ground state would yield only a single line. We consider that the nearest that could belong to the Gd^{3+} spectrum in the present work is the one discussed above (b1–b5) with extreme fine structure lines ($\pm 7/2 \leftrightarrow \pm 5/2$ transitions) not being seen due to very low intensity. However, we have not assigned spectrum b1–b5 to Gd^{3+}, as the spectrum appeared clearly only in irradiated samples.

4.2. Dose dependence

To the best of our knowledge, the only case of dose dependence of EPR line position has been for neutron irradiated graphite [27, 28]. This was explained as a consequence of interaction of conduction electrons with the radiation induced static paramagnetic centers. As the interaction is dynamic, the effective g-value is a weighted average of g-values of all the interacting species. The number of paramagnetic centers increases with increase of dose, and consequently the g-value shifts towards the value of an isolated static paramagnetic center in graphite. In an intrinsic semiconductor uranium molybdenum sulfide [29], the physical nature of such an interaction of the static paramagnetic center with conduction electrons was invoked to explain the large temperature dependence in the position of the U^{4+} line. With increasing temperature, the conduction/mobile electron density increased and the g-value shifted towards 2.00. In general, systems with significant concentrations of unlike spins (through exchange interaction) exhibit electron magnetic resonance lines at effective g-values. These depend on the relative concentrations of individual magnetic ions. Different manifestations of exchange interactions in the EPR spectra are discussed by Bencini and Gatteschi [30]. Skrzpek and Bialas-Borg [31] have shown the g_{eff} in a system containing magnetic ions with different g-values; (a) depends on the relative concentrations of the magnetic ions, and (b) follows the predictions of Huber's theory for exchange coupled systems with unlike spins [32]. They have shown that g_{eff} of a single line EPR of magnetically coupled divalent Mn and Ni ions in $KNi_xMn_{1-x}F_3$ depends on the value of 'x'. The Mn^{2+} ion with $3d^5$ outer electron configuration and ^6S ground state is a Kramers' ion with its EPR easily observable at room temperature. On the other hand, the Ni^{2+} ion with $3d^8$ outer electron configuration with $S = 1$ in the ground state is a non-Kramers' ion, with its EPR normally observable only at lower temperatures due to strong spin–lattice interaction. In $K(Mn,Ni)F_3$, a single line EPR was observed at room temperature with g_{eff} that was dependent on the concentration of the coupled magnetic ions, satisfying the equation

$$g_{\text{eff}} = [g_{\text{Mn}} S_{\text{Mn}}(S_{\text{Mn}} + 1)N_{\text{Mn}} + g_{\text{Ni}} S_{\text{Ni}}(S_{\text{Ni}} + 1)N_{\text{Ni}}]/[S_{\text{Mn}}(S_{\text{Mn}} + 1)N_{\text{Mn}} + S_{\text{Ni}}(S_{\text{Ni}} + 1)N_{\text{Ni}}]. \quad (1)$$

In the present case, the most likely centers which can be exchange coupled are the trapped hole center O^-, which can have a 'hopping electron' at room temperature, and Fe^{2+} and Fe^{3+}. Divalent Mn was present in only one sample. It is known that iron exhibits multiple valence, the predominant states being Fe^{2+}, Fe^{3+}, and Fe^{4+}. Earlier work on Fe^{3+} centers in quartz has shown that Fe^{3+} enters the lattice at the Si^{4+} site and this should be the case for feldspars. In view of the oxygen sharing of adjacent SiO_4 tetrahedra, the ferric complex is described as $(FeO_4)^-$. It was shown by Choi and Weil [11] that such a complex bound to charge compensating monovalent alkali cations takes part in a correlated motion with hopping 'holes' on oxygens. In view of the appreciable delocalization of spin density on to the neighboring ions, Weil [8] suggested that it is reasonable to consider resonant forms of the type $Fe^{3+}O^{2-}$ and $Fe^{2+}O^-$ for the ferric complex. We examined the scenario wherein the iron center at tetrahedral sites in feldspars resonates between these two states, resulting in an averaged spectrum. The interaction with O^- centers was subsequently introduced to account for the dose dependence of the line. We also considered the fast electron exchange between Fe^{2+} at the Ca site and Fe^{3+} at the adjacent T1m or T10 site. The effective g for these species was obtained from equation (1) using the appropriate g-values for the respective species given in table 4a. The species, their expected g-values, and the experimental observations wherever available are collated in table 4b. When the system resonates between $Fe^{2+}O^-$ and $Fe^{3+}O^{2-}$ at a frequency greater than the difference in their

Table 4a. The basic data used in the calculation of g_{eff} for different possible Fe^{3+}–Fe^{2+}–O^- species.

Parameter	Fe^{3+}/Fe^{3+}–O^{2-}	Fe^{2+}	O^-	Fe^{2+}–O^-
S	5/2	2	1/2	3/2
g	2.003	3.54	2.03	3.271
$S(S+1)$	35/4	6	3/4	15/4
$gS(S+1)$	35/2	20.58	1.5225	12.27

Table 4b. The g_{eff}-values for different Fe^{3+}–Fe^{2+}–O^- species.

Species	g_{eff} (calculated)	Experimental	
		g-value	Sample
Fe^{2+}–O^- ↔ Fe^{3+}–O^{2-} resonant forms	2.635	2.689 2.774	Dz-2 Dz-4
Exchange coupled Fe^{3+} and Fe^{2+}	2.5817	—	—
Exchange coupled			
Fe^{3+}–Fe^{2+}–O^-	2.555	2.545	GP-3
Fe^{3+}–Fe^{2+}–$2O^-$	2.5304		Y-7A TML-1
Fe^{3+}–Fe^{2+}–$3O^-$	2.508		
Fe^{3+}–Fe^{2+}–$4O^-$	2.488	2.432	Y7A (200 Gy)

Zeeman splitting, i.e. $(g_{Fe^{2+}}-g_{Fe^{3+}})\beta H$, and the respective zero field splitting, a single line can be expected at a g-value of 2.635. This is close to the g_{eff}-values in samples Dz-2 and Dz-4. The exchange coupled Fe^{3+} and Fe^{2+} are expected to give a single line at $g = 2.5817$, and none of the observed lines matched this. Interestingly, the exchange coupling between Fe^{3+}, Fe^{2+}, and O^- had $g_{\text{eff}} = 2.555$, and if another O^- were also included the g-value would decrease to 2.535. Both these values are close to the observed value of $g_{\text{eff}} = 2.545$ in samples GP-3, Y7A and sun bleached TML-1. With radiation dose, the number density of O^- increases and the g-value of the exchange coupled system decreases. It nearly follows the dose dependence of the line position. This suggests that the holes on O^- at room temperature are strongly coupled to both ferrous and ferric ions. It may be remarked that exchange coupled metal ions and their interaction with 'holes' on oxygen are not unknown in feldspars. The blue to bluish green color of amazonite, a variety of microcline, was attributed to an absorption band at 630 nm due to the formation of exchange coupled Pb^+–O–Fe^{3+} complexes, causing a significant increase in the intensity of the $^4A_1 \rightarrow {}^4T_1$ transition of Fe^{3+} [33]. Further, among the samples investigated, the $g_{\text{eff}} = 2.54$ line was observed in TML-1 only after exposure of the samples to daylight. In these samples the Mn impurity at the 20–40 ppm level exists in divalent form as seen by EPR. At this stage, it can only be conjectured that divalent Mn, being a highly stable species, probably suppressed the formation of divalent Fe, thereby $Fe^{3+}O^{2-} \leftrightarrow Fe^{2+}O^-$. The exposure to light appears to have generated some O^- species close to Fe centers, triggering the formation of exchange coupled units, resulting in the $g_{\text{eff}} = 2.545$ line.

For averaging of g-values between two or more exchange coupled species (as in the case of interacting Mn and Ni or Fe^{3+} and Fe^{2+}, or even Fe^{3+}–Fe^{2+}–O^-), there is no need to invoke mobile paramagnetic species. However, when considering the radiation induced defects interacting with a dilute paramagnetic center such as Fe^{3+} of fixed concentration, and to account for the dose dependent (i.e. concentration dependent, in real terms) g_{eff}, we have a situation wherein Fe^{3+} interacts with more than one O^-. The probability that a given Fe^{3+} has more than one static O^- in its proximity would be small and it would be insignificant for each additional O^-. We have therefore invoked mobile O^- in analogy with neutron irradiated graphite [26, 27], wherein interaction between itinerant conduction electrons and static free radicals resulted in dose dependent line position. The existence and feasibility of mobile 'holes' on O^- in silicates is well established by the EPR work of Choi and Weil [11] in alkali containing alpha-quartz.

5. Conclusions

(1) An unusual EPR line detected in the $g = 2.5$–2.6 region in feldspars is reported for the first time.
(2) It is suggested that this line is due to an exchange interaction between ferrous and ferric impurities and hopping trapped hole center O^-. This results in two situations, one of them a flip–flop between two resonant forms $Fe^{3+}O^{2-} \leftrightarrow Fe^{2+}O^-$ and the other an exchange coupled Fe^{3+}–Fe^{2+}–O^-. Being the weighted average of the interacting paramagnetic species, the position of this line changes with gamma dose due to an increase in the number of oxygen 'hole' centers.
(3) Given the high precision of the g-value measurements in modern ESR systems, we conjecture the use of the dose dependence of the $g_{\text{eff}} = 2.54$ line for radiation dosimetry and geochronology. Simple calculations suggest that sub-gray precision corresponding to an age resolution on a century scale should be possible. This aspect will be examined in a future report.

Acknowledgments

We are grateful to Professors M Lamothe, M Auclair, E Derbyshire and R Kemp for the samples. We wish to thank the Director of the National Geophysical Research Institute, Dr V P Dimri, for his kind encouragement and permission to use NGRI, ICPMS facility. We thank the editors and the referees for their constructive suggestions.

References

[1] Krbetschek M R, Gitze J, Dietrich A and Trautmann T 1997 *Radiat. Meas.* **27** 695–748
[2] Gaines R V, Skinner H C W, Foord E, Mason B and Rosenzweig A 1997 *Dana's New Mineralogy* (New York: Wiley) p 1819
[3] Weeks R A J 1973 *Geophys. Res. Lett.* **78** 2393–401
[4] Speit B and Lehmann G 1982 *Phys. Chem. Minerals* **8** 77–82
[5] Hofmeister A M and Rossmann G R 1984 *Phys. Chem. Minerals* **11** 213–24

[6] Petrov I and Hafner S S 1988 *Am. Mineral.* **73** 87–104
[7] Finch A A and Klein J 1999 *Contrib. Mineral. Petrol* **135** 234–43
[8] Weil J A 1984 *Phys. Chem. Minerals* **10** 149–65
[9] Minge J, Mombourquette M J and Weil J A 1989 *Phys. Rev* B **40** 6523–8
[10] Minge J, Mombourquette M J and Weil J A 1990 *Phys. Rev.* B **42** 33–6
[11] Choi D and Weil J A 1990 *Phys. Rev.* B **42** 9759–65
[12] Upadrashta Y and Weil J A 2002 A compendium of EPR spectra arising from various paramagnetic defects in powdered alpha-quartz *Technical Report* (Saskatoon, Canada: University of Saskatchewan)
[13] Lees N S, Walsby C J, Williams J A S, Weil J A and Claridge R F C 2003 *Phys. Chem. Minerals* **30** 131–41
[14] Castner T, Newell G S, Holton W C and Slichter C P 1960 *J. Chem. Phys.* **32** 668
[15] Abragam A and Bleaney B 1971 *Paramagnetic Resonance of Transition Ions* (Oxford: Clarendon) pp 203–5
[16] Ikeya M 1993 *New Application of Electron Spin Resonance Dating, Dosimetry and Microscopy* (Singapore: World Scientific) p 500
[17] Subramanian S, Murty P N and Murty C R K 1977 *J. Magn. Reson.* **25** 101–10
[18] Jimin S 2002 *Earth Planet. Sci. Lett.* **203** 845–59
[19] Zahida B, Balaram V, Ahmad S M, Satyanarayanan M and Ganeshwar R 2007 *At. Spectrosc.* **28** 41–50
[20] Poolton N R J, Nicholls J E, Botter-Jensen L, Smith G M and Reidi P C 2001 *Phys. Status Solidi* b **225** 467–75
[21] Weil J A, Bolton J R and Wertz J E 1994 *Electron Paramagnetic Resonance: Elementary Theory and Practical Applications* (New York: Wiley)
[22] Rappaz M, Abraham M M, Ramey J O and Boatner L A 1981 *Phys. Rev.* B **23** 1012–30
[23] Geshwind S and Remeika J P 1961 *Phys. Rev.* **122** 757
[24] Low W and Zusman A 1963 *Phys. Rev.* **130** 144
[25] Low W 1956 *Phys. Rev.* **101** 1827–8
[26] Sastry M D 1976 *Phys. Rev.* B **13** 156
[27] Arnold G and Mrozowski S 1968 *Carbon* **6** 243–56
[28] Mizushima S 1968 *Carbon* **6** 13
[29] Kadam R M, Sastry M D, Iyer R M, Gopalakrishnan I K and Yakhmi J V 1997 *Phil. Mag.* B **75** 503–8
[30] Bencini A and Gatteschi D 1990 *Electron Paramagnetic Resonance of Exchange Coupled Systems* (Berlin: Springer) p 287
[31] Skrzypek D and Bialas-Borge K 1980 *J. Phys. C: Solid State Phys.* **21** 1807–14
[32] Huber D L 1975 *Phys. Rev.* B **12** 31–8
[33] Petrov I, Mineeva R M, Bershov L V and Agel A 1993 *Am. Mineral.* **78** 500–10
[34] Griscom D L 1973 *J. Non-Cryst. Solids* **8** 251–85